Drivers of cloud droplet number variability in the summertime Southeast United States

Aikaterini Bougiatioti[1,2], Athanasios Nenes[2,3,4], Jack J. Lin[2,a], Charles A. Brock[5], Joost A. de Gouw[5,6,b], Jin Liao[5,6,c,d], Ann M. Middlebrook[5], André Welti[5,6,e]

[1]Institute for Environmental Research & Sustainable Development, National Observatory of Athens, P. Penteli, GR-15236, Greece
[2]School of Earth & Atmospheric Sciences, Georgia Institute of Technology, Atlanta, GA 30332, USA
[3]Laboratory of Atmospheric Processes and their Impacts, School of Architecture, Civil & Environmental Engineering, École Polytechnique Fédérale de Lausanne, CH-1015, Lausanne, Switzerland
[4]Institute for Chemical Engineering Sciences, Foundation for Research and Technology Hellas, Patras, GR-26504, Greece
[5]Chemical Sciences Division, NOAA Earth System Research Laboratory, Boulder, CO, 80305, USA
[6]Cooperative Institute for Research in Environmental Sciences, Univ. of Colorado, Boulder, CO, 80309, USA
[a] now at: Nano and Molecular Systems Research Unit, Box 3000, FI-90014 University of Oulu, Oulu, Finland
[b] now at: Department of Chemistry and Biochemistry, University of Colorado Boulder, Boulder, CO, USA
[c] now at: Atmospheric Chemistry and Dynamic Laboratory, NASA Goddard Space Flight Center, Greenbelt, MD, USA
[d] now at: Universities Space Research Association, GESTAR, Columbia, MD, USA
[e] now at: Atmospheric Composition Research Unit, Finnish Meteorological Institute, Helsinki, Finland

Correspondence to: Aikaterini Bougiatioti (abougiat@noa.gr), Athanasios Nenes (athanasios.nenes@epfl.ch).

Abstract

The Southeast United States has experienced a different climate warming trend compared to other places worldwide. Several hypotheses have been proposed to explain this trend, one being the interaction of anthropogenic and biogenic aerosol precursors that synergistically promote aerosol formation, elevate cloud droplet concentration and induce regional cooling. We examine these aerosol-cloud droplet links by analyzing regional scale data collected onboard the NOAA WP-3D aircraft during the 2013 Southeast Nexus (SENEX) campaign to quantify the sensitivity of droplet number to aerosol number, chemical composition and vertical velocity on a regional scale. The observed aerosol size distributions, chemical composition and vertical velocity distribution (Gaussian with standard deviation σ_w) are introduced into a state-of-the-art cloud droplet parameterization to show that cloud maximum supersaturations in the region are low, ranging from 0.02 to 0.52% with an average of 0.14±0.05%. Based on these low values of supersaturation, the majority of activated droplets correspond to particles of diameter 90 nm and above. Droplet number shows little sensitivity to total aerosol owing to their strong competition for water vapor. Given, however, that σ_w exhibits considerable diurnal variability (ranging from 0.16 m s^{-1} during nighttime to over 1.2 m s^{-1} during day), its covariance with total aerosol number (N_a) during the same period amplifies

39   predicted response in cloud droplet number (N_d) by 3 to 5 times. Therefore, correct consideration of vertical

40   velocity and its covariance with time and aerosol amount is important for fully understanding aerosol-cloud

41   interactions and the magnitude of the aerosol indirect effect. Datasets and analysis such as the one presented

42   here can provide the required constraints for addressing this important problem.

43

44   **1. Introduction**

45   Atmospheric particles (aerosols) interact with the incoming solar radiation through scattering and

46   absorption processes which tend to cool the Earth, especially over dark surfaces such as oceans and forests

47   (Brock et al., 2016a). Aerosols also act as cloud condensation nuclei (CCN) and subsequently form cloud

48   droplets and indirectly affect climate through modification of cloud radiative properties - an effect which

49   constitutes one of the most uncertain aspects of anthropogenic climate change (Seinfeld et al., 2016).

50   Studies often highlight the importance of constraining the aerosol size distribution, particle composition

51   and mixing state for predicting CCN concentrations (Cubison et al., 2008; Quinn et al., 2008). Model

52   assumptions often cannot consider the full complexity required to comprehensively compute CCN – which

53   together with other emissions and process uncertainties lead to CCN prediction errors that can be significant

54   (e.g., Fanourgakis et al., 2019). Owing to the sublinear response of cloud droplet number concentration (N_d)

55   to aerosol perturbations, prediction errors in CCN generally result in errors in N_d which are less than those

56   for CCN (Fanourgakis et al., 2019). The sublinear response arises because elevated CCN concentration

57   generally increases the competition of the potential droplets for water vapor; this in turn depletes

58   supersaturation and the N_d that can eventually form (Reutter et al., 2009; Bougiatioti et al., 2016;

59   Fanourgakis et al., 2019; Kalkavouras et al., 2019). A critically important parameter is the vertical velocity;

60   so important in fact that droplet number variability may be driven primarily by vertical velocity variations

61   (Kacarab et al., 2020; Sullivan et al., 2019). Compared to aerosols, vertical velocity is much less observed,

62   constrained and evaluated in aerosol-cloud interaction studies, hence may be a source of persistent biases

63   in models (Sullivan et al., 2019).

64   The Southeast United States (SEUS) presents a particularly interesting location for studying regional

65   climate change, as it has not considerably warmed over the past 100 years – except for the last decade

66   (Carlton et al., 2018; Yu et al., 2014; Leibensperger et al., 2012b). These trends are in contrast with the

67   trends observed in most locations globally (IPCC 2013), and several hypotheses have been proposed to

68   explain this regional phenomenon, including the effect of involving short-lived climate forcers such as

69   secondary aerosols combined with the enhanced humidity in the region and their impact on clouds (Carlton

70   et al., 2018; Yu et al., 2014). Here, we analyze data collected during the Southeast Nexus of Air Quality

71   and Climate (SENEX) campaign in June-July 2013, which was the airborne component led by the National

72   Oceanic and Atmospheric Administration (NOAA), of a greater measurement campaign throughout the

73   SEUS, the Southeast Atmosphere Study (SAS; Carlton et al., 2018). Here we analyze data collected onboard

74   the NOAA WP-3D and apply a state-of-the-art droplet parameterization to determine the maximum

75   supersaturation and N_d achieved in cloudy updrafts, for all science flights with available number size

76   distribution and chemical composition data. We also determine the sensitivity of droplet formation to

77   vertical velocity and aerosol, with the purpose of understanding the drivers of droplet variability in the

78   boundary layer of the SEUS by obtaining regional-scale, representative values of the relationship between

79   the driving parameters and cloud droplet number.

80

81   **2. Methods**

82   *2.1 Aircraft instrumentation*

83   The analysis utilizes airborne, in situ data collected during the June-July 2013 SENEX mission, aboard the

84   National Oceanic and Atmospheric Administration (NOAA) WP-3D aircraft (typical airspeed ~100 m s^{-1})

85   based in Smyrna, Tennessee (36º00'32''N, 86º31'12''W). In total, twenty research flights were conducted.

86   Based on the availability of the relevant data described below, thirteen flights are analyzed in this work.

87   Description of the analyzed research flights are provided in Table 1. Detailed information on the

88   instrumentation and measurement strategy during the SENEX campaign can be found in Warneke et al.

89   (2016).

90   Dry particle number distributions from 4 - 7000 nm were measured using multiple condensation and optical

91   particle counters. 4-700 nm particles were measured by a nucleation mode aerosol size spectrometer

92   (NMASS; Warneke et al., 2016) and an ultra-high sensitivity aerosol spectrometer (UHSA; Brock et al.,

93   2011), while for larger particles with dry diameters between 0.7 and 7.0 μm, a custom-built white-light

94   optical particle counter (WLOPC) was used.

95   Measurements of the composition of submicron vacuum aerodynamic diameter non-refractory aerosol (less

96   than 0.7 μm diameter) were made with a Compact Time-of-Flight Aerosol Mass Spectrometer (C-ToF-

97   AMS; Aerodyne, Billerica, Massachesetts, US) (Canagaratna et al., 2007; Kupc et al., 2018) customized

98   for aircraft use, with a 10 s time resolution (Warneke et al., 2016). Particles entering the instrument are

99   focused and impacted on a 600 ºC inverted-cone vaporizer. The volatilized vapors are analyzed by electron

100 ionization mass spectrometry, providing mass loadings of sulfate, nitrate, organics, ammonium and

101 chloride. For the C-ToF-AMS, the transmission efficiency of particles between 100 and 700 nm is assumed

102 to be 100% through the specific aerodynamic focusing lens used while mass concentrations are calculated

103 using a chemical composition-dependent collection efficiency (Middlebrook et al., 2012; Wagner et al.,

104 2015). The C-ToF-AMS only measures non-refractory aerosol chemical composition, therefore this

105 analysis provides mass loadings of sulfate, nitrate, ammonium and organic constituents with a 10 s time

106 resolution and neglects the contribution of black carbon (BC). The calculation of the average volume

107 fractions from the mass loading follows that of Moore et al. (2012). An average organic density of 1.4 g

108 cm^{-3} is used, characteristic of aged aerosol (Moore et al., 2011; Lathem et al., 2013) while for the inorganic

109 species the respective densities are used, assuming the aerosol to be internally mixed.

110 The aircraft was equipped by the NOAA Aircraft Operations Center (AOC) flight facility, incorporating a

111 suite of instruments to provide information on exact aircraft position as well as numerous meteorological

112 parameters (Warneke et al., 2016). The analysis in this work makes use of vertical wind velocity, aircraft

113 radar altitude, and ambient temperature, pressure and relative humidity (RH) provided by NOAA AOC.

114 Location of the instrumentation on the aircraft can be found elsewhere (Warneke et al., 2016). For

115 measurements inside the fuselage a low turbulence inlet (Wilson et al., 2004) and sampling system (Brock

116 et al., 2011; 2016a) was used to decelerate the sample flow to the instruments. The C-ToF-AMS was

117 connected downstream of an impactor with 50% efficiency at a 1.0 μm aerodynamic diameter (PM1) cut-

118 point (Warneke et al., 2016).

119 *2.2 Aerosol hygroscopicity parameter*

120 The aerosol hygroscopicity parameter (Petters and Kreidenweis, 2007), κ, is calculated assuming a mixture

121 of an organic and inorganic component with volume fraction ε_{org}, ε_{inorg} and characteristic hygroscopicity

122 κ_{org}, $\kappa_{inorg,}$ respectively ($\kappa=\varepsilon_{inorg}\kappa_{inorg}+\varepsilon_{org}\kappa_{org}$). The organic and inorganic volume fraction are derived from

123 the C-ToF-AMS data. Since throughout the summertime SEUS, aerosol inorganic nitrate mass and volume

124 fraction are very low (Weber et al., 2016; Fry et al., 2018), κ_{inorg} =0.6, representative for ammonium sulfate,

125 is used. For the organic fraction, a hygroscopicity value of κ_{org}=0.14 is used, based on concurrent

126 measurements conducted at the ground site of the SAS at the rural site of Centreville, Alabama (Cerully et

127 al., 2015). This value is also in accordance with the cumulative result of studies conducted in the Southeast

128 US using measurements of droplet activation diameters in subsaturated regimes, providing κ_{org} of > 0.1

129 (Brock et al., 2016a).

130 *2.3 Cloud droplet number and maximum supersaturation*

131 Using the observed aerosol number size distribution (1 s time resolution) and the hygroscopicity derived

132 from the chemical composition measurements (10 s time resolution), we calculate the droplet number (N_d)

133 and maximum supersaturation (S_{max}) that would form in clouds in the airmasses sampled. Droplet number

134 and maximum supersaturation calculations are carried out at a regional scale using an approach similar to

135 that of Bougiatioti et al. (2016) and Kalkavouras et al. (2019) with the sectional parameterization of Nenes

136 and Seinfeld (2003), later improved by Barahona et al. (2010) and Morales Betancourt and Nenes (2014a).

137 A sectional representation of the size distribution is used and provided for each data point of each flight

138 (per second, e.g. for Flight 5, n=23213 data points). Given that chemical composition is provided with a 10

139 s time resolution, the same hygroscopicity values are used for 10 size distributions during each flight.

140 Temperature and pressure required for droplet number calculations are obtained from the NOAA AOC

141 flight facility dataset.

142 Droplets form from activation of aerosol in cloudy updrafts, so here we use the available measurements of

143 vertical velocity together with the aerosol measurements to derive a potential cloud droplet concentration.

144 Given that vertical velocity varies considerably inside the boundary layer we represent droplet number with

145 the average concentration that results from integrating over the distribution (probability density function,

146 PDF) of observed updraft velocities. To accomplish this, each flight is divided in segments where the

147 aircraft flew at a constant height. For each segment, the positive vertical velocities are fit to a Gaussian

148 distribution with mean of zero and width of spectral dispersion σ_w. Positive vertical velocities ("updrafts")

149 were used, as they are the part of the vertical velocity spectrum that is responsible for cloud droplet

150 formation. The σ_w values derived from the level leg segments are then averaged into one single σ_w value

151 (and standard deviation) to represent the flight. Application of the "characteristic velocity" approach

152 (Morales and Nenes, 2010) then gives the PDF-averaged droplet number concentration by calling the

153 droplet parameterization at a single "characteristic" velocity, $w^* = 0.79\sigma_w$ (Morales and Nenes, 2010). This

154 calculation approach is applied to each size distribution measured. Apart from its theoretical basis, this

155 methodology has shown to provide closure with observed droplet numbers in ambient clouds (e.g. Kacarab

156 et al., 2020).

157 In determining σ_w, we consider segments that are expected to be in the boundary layer: 91 % of the segments

158 are below 1000 m (mean altitude ~700 m; Table 2) typically corresponding to the height of the boundary

159 layer in the summertime US (Seidel et al., 2013). The vertical velocity distributions observed gave σ_w

160 $=0.97\pm0.21$ m s^{-1} for daytime flights, and σ_w $=0.23\pm0.04$ m s^{-1} for nighttime flights (Table 2). Because of

161 this strong diurnal variation in σ_w, potential droplet formation is evaluated at four vertical velocities that

162 cover the observed ranged, namely 0.1, 0.3, 0.6 and 1 m s^{-1}.

163 We also compute the sensitivity of the derived N_d, to changes in aerosol number concentration (N_a), κ and

164 σ_w, expressed by the partial derivatives $\partial N_d/\partial N_a$, $\partial N_d/\partial \kappa$ and $\partial N_d/\partial \sigma_w$ computed from the parameterization

165 using a finite difference approximation (Bougiatioti et al., 2016; Kalkavouras et al., 2019). These

166 sensitivities, together with the observed variance in N_a, κ, and σ_w are also used to attribute droplet number

167 variability to variations in the respective aerosol and vertical velocity parameters following the approach

168 of Bougiatioti et al. (2016) and Kalkavouras et al. (2019).

169

170 **3. Results and Discussion**

171 *3.1. Particle composition and size distribution*

172 For the determination of the different aerosol species present, neutral and acidic sulfate species are

173 distinguished by the molar ratio of ammonium to sulfate ions. A molar ratio higher than 2 indicates the

174 presence of only ammonium sulfate, while values between 1 and 2 indicate the presence of both ammonium

175 sulfate and bisulfate (Seinfeld and Pandis, 1998). For most of the flights, the molar ratio of ammonium

176 versus sulfate was well above 2, having a mean value of 2.41±0.72 (median 2.06). For the nighttime flights

177 the values were somewhat lower (1.91±0.42 and median of 1.85, respectively). Nevertheless, ammonium

178 sulfate is always the predominant sulfate salt. Organic mass fractions for the SENEX research flights are

179 provided in Table 1. Overall, organic aerosol was found to dominate during all flights, contributing 66%-

180 75% of the total aerosol volume. Most of the remaining aerosol volume consists of ammonium sulfate,

181 ranging from 12%-39% (with a mean of 23%±6%). The organic mass fraction during the flights was found

182 to decrease with height (see Fig. 1). This vertical variability of the chemical composition can have a strong

183 impact on droplet number within the boundary layer, as air masses from aloft may descend and interact

184 with that underneath. Figure 1 represents the organic mass fractions during Flights 5 and 12. The lowest

185 organic mass fractions overall were observed during Flight 12 (35%±18% with values < 5% for altitudes

186 >3000 m, Fig.1b) while the highest ones were observed at flights over predominantly rural areas (Flights 5

187 (Fig. 1c) , 10 and 16). During Flight 5 the organic mass fraction was high (68%±5%), with the highest

188 values found in the free troposphere at altitudes > 3000 m. High organic mass fractions were also found

189 during a nighttime flight that included portions of the Atlanta metropolitan area, with values up to 78%.

190 The impact of the chemical variability on droplet number is discussed in section 3.2.

191 The predominance of the organic fraction is also reflected in the hygroscopicity parameter values, with an

192 overall $\kappa = 0.25\pm0.05$, which is close to the proposed global average of 0.3 (Seinfeld and Pandis, 1998).

193 The highest values are, as expected, for flights exhibiting the lowest organic mass fraction, namely Flight

194 12 with a $\kappa = 0.39$ (Table 2). The rest of the κ-values are close to the overall values, as the organic mass

195 fractions are around 0.65.

196 Median aerosol size distributions are obtained from the median and interquartile range in each size bin from

197 the aerosol size distribution measurements during segments where the aircraft flew at a constant height.

198 The impact of the variability of the total aerosol number on droplet number is discussed in detail further in

199 section 3.2. Overall, number concentrations ranged from around 500 to over 100000 cm^{-3} with number size

200 distributions varying markedly over the course of a flight. In general, free tropospheric distributions

201 exhibited characteristics of a bimodal distribution with a prominent broad accumulation mode peak (80-

202 200 nm) and an Aitken mode peak (30-60 nm) (Fig. 2a) while boundary layer size distributions exhibited a

203 more prominent accumulation mode (Fig. 2b). There was considerable variability in the contributions of

204 the nucleation, Aitken, and accumulation modes to the total aerosol number, depending on altitude and

205 proximity to aerosol sources (Fig. 2c). Nevertheless, the modal diameters did not vary much. Distributions

206 during nighttime flights exhibited similar total aerosol number and variability; nevertheless, size

207 distributions were more complex exhibiting even three different modes (20-40, 70-100 and 130-200 nm;

208 Fig. 2d). Considering that mostly particles in the accumulation mode activate into cloud droplets (particles

209 with diameters >90 nm), contrasts between day and nighttime aerosol characteristics/variability may not be

210 as large, and driven primarily by the total aerosol number in the accumulation mode.

211 *3.2 Potential cloud droplet number*

212 The calculation of N_d and S_{max}, was carried out for all thirteen research flights. Results are given in Tab. 3

213 for the four different values (0.1, 0.3, 0.6 and 1 m s^{-1}) of σ_w. Overall it can be seen that for all flight

214 conditions and for low σ_w, N_d shows a low variance (mean of 132±20 for 0.1 m s^{-1} and 350±100 for 0.3 m

215 s^{-1}). For a given σ_w, the variance of N_d is predominantly attributed to relative changes in N_a rather than

216 changes in the chemical composition (expressed by changes in the hygroscopicity parameter, κ). The

217 highest relative contribution of the chemical composition (12% and 35% for 0.1 and 0.3 m s^{-1}, respectively)

218 to the variation of N_d is found for Flight 18, during which the total aerosol number was the lowest. Indicative

219 of a "cleaner" environment; the organic mass fraction was relatively lower and the hygroscopicity

220 parameter was higher. Even though the lowest organics mass fraction and highest κ were observed during

221 Flight 12, droplet formation is much more sensitive to changes in aerosol concentration than to variations

222 in composition.

223 As the vertical velocity increases, so does supersaturation and consequently the droplet number (by 62%

224 from 0.1 to 0.3 m s^{-1}, 70% from 0.3 to 0.6 m s^{-1} and another 39% from 0.6 to 1 m s^{-1}). The relative

225 contribution of the chemical composition to the variation of cloud droplet number increases from 5±3% for

226 0.1 m s^{-1}, to 12.3±8% for 0.3 m s^{-1}, to 14.5±10% for 0.3 m s^{-1} and 16.5±9% for 1 m s^{-1}. The highest droplet

227 numbers are estimated for Flights 6 and 10, which included urban environments during daytime (Atlanta).

228 Overall during daytime, when σ_w varies little and is large, and N_a is high, the relative contribution of N_a to

229 the variation of N_d is the highest (more than 90%) while the relative contribution of κ is limited (less than

230 10%) (see Table 3, Flights 10, 11, 12, 17 and 19). Turbulence is limited during nighttime when σ_w is the

Atmospheric
Chemistry
and Physics
Discussions

231   lowest (0.23±0.04); therefore, the $\sigma_w = 0.3$ m s^{-1} case is most representative of nighttime conditions. During

232   daytime, when σ_w is high (0.97±0.21), $\sigma_w = 1$ m s^{-1} should be considered as most representative.

233   As σ_w varies considerably throughout the day, we estimate its contribution together with variations in N_a

234   and κ, to the total variability in N_d based on $\partial N_d/\partial \kappa$, $\partial N_d/\partial N_a$ and $\partial N_d/\partial \sigma_w$ and the variances of κ, N_a and σ_w

235   (Table 4). The σ_w variation during nighttime, although small (always less than 10%), consistently remains

236   an important contributor to N_d variability, because droplet formation tends to be in the updraft velocity-

237   limited regime. At higher values of σ_w (Table 4), the contribution of σ_w variability to $\underline{N_d}$ variability is reduced

238   and dominated by N_a variability.

239   To explore the importance of aerosol compared to updraft velocity, we focus on two pairs of flights

240   conducted in two sectors, from each sector one during day- and one during night-time (see Fig.3). In both

241   pairs of flights (Flight 5 and 15, and Flight 6 and 9), σ_w varies about the same between night and day (Table

242   4). For the first pair of flights, the daytime variability in N_d (which is 69%) is to within 75% driven by

243   aerosol (69% by N_a and 7% from κ) and 24% by σ_w. For nighttime, 58% by aerosol (51% by N_a and 7%

244   from κ) and 42% of the variability is driven by σ_w. For the second pair of night/day flights, N_a is on average

245   similar, σ_w varies by a factor of 4.0 and κ varies by 13%. Attribution calculations suggest that the diurnal

246   variability in N_d (where daytime values are 72.1% higher than nighttime) is 3, 54 and 43% for κ, N_a and σ_w,

247   respectively during day and 7, 76, and 17% driven by κ, N_a and σ_w, respectively during night (Table 4). In

248   the second sector, 57% of the variability in N_d is driven by aerosol during the day and 83% during the night.

249   As expected, droplet number (N_d) and maximum supersaturation (S_{max}) increases as σ_w becomes larger. The

250   highest S_{max} are around 0.2-0.3% and found for flights which exhibited large and highly variable σ_w (Flights

251   4, 5, 12 and 19) while the lowest S_{max} are around 0.10% and found for the nighttime flights (Flights 9, 15

252   and 16). All other flights yield similar S_{max}, which are around 0.13%. Based on the calculated S_{max} for every

253   flight, the majority of the activated droplets correspond to particles of 90 nm diameter and above. Figure 3

254   presents the calculated N_d for the four aforementioned flights, namely Fights 5 (Fig. 3a), 15 (Fig. 3b), 6

255   (Fig. 3c) and 9 (Fig. 3d) using the observed σ_w. The size of the markers represents the number of droplets,

256   while the color scale the respective total aerosol number.

257   Figure 4 shows N_d relative to N_a for flights conducted in two sectors, during day and night (Flights 5 & 15,

258   and Flights 6 & 9, respectively). It can be seen that throughout these flights, N_d reaches a plateau, where

259   any additional aerosol does not translate to any significant increase in N_d. This plateau is caused by strong

260   water vapor limitations and is different for day and night. S_{max} is lower during night because vertical wind

261   velocity, ambient T and RH are lower. The same factors cause that for Flight 6 & 9 (Fig. 4c & d) where N_a

262   was almost the same, N_d is almost 3.5 times lower during night (Flight 9). For the whole dataset (13 flights),

263   results are summarized in Figure 5, where droplet numbers are calculated based on the observed σ_w and the

264   respective "characteristic", mean velocities, $w*$. Under low $w*$ conditions, N_a variability does not result in

265   an important change in N_d. On the contrary, when $w*$ tends to increase and N_a increases, as is characteristic

266   of polluted regions, during daytime, then the impact on droplet number is more notable. This point is evident

267   in Figure 6, comprising the different segments of the flights when the aircraft sampled at practically the

268   same altitude within the boundary layer. It can be seen that N_a is enhanced as $w*$ increases. The lowest $w*$

269   values (shaded area) correspond to the segments of the flights during nighttime.

270   Overall, S_{max} of clouds from all the evaluated SENEX data, is 0.14±0.05%. Tripling σ_w from 0.1 to 0.3 m s$^-$

271   ^{1} results in 31% increase in S_{max}, while doubling from 0.3 to 0.6 m s^{-1} results in 26.2% increase in S_{max} and

272   a further σ_w increase to 1 m s^{-1} leads to an additional 20.7% increase in S_{max}. Overall effect of updraft

273   velocity on calculated N_d: tripling σ_w from 0.1 to 0.3 m s^{-1} results in a 61.9% increase in N_d, doubling from

274   0.3 to 0.6 m s^{-1} results in 40.5% N_d increase; increasing σ_w to 1 m s^{-1} leads to an additional 26.9% increase

275   in N_d. Furthermore, for a given σ_w, despite of the presence or not of a large number of aerosol (e.g. Flight

276   10 where N_a is 2.7 times higher than N_a in Flight 15) the difference in calculated N_d for 0.6 m s^{-1} is only 1.3

277   times higher for Flight 10 than Flight 15. This highlights the relative insensitivity of N_d to variations in N_a

278   for constant σ_w.

279

280   4. Summary and Conclusions

281   Measurements of wind velocity, ambient conditions (*T, RH*), aerosol number size distribution and

282   composition in the SEUS obtained during the SENEX 2013 project are used to analyze the drivers of droplet

283   formation. Overall 13 research flights are studied, covering environments over sectors with different aerosol

284   sources, impacting total aerosol number, size distribution and chemical composition. Aerosol volume is

285   largely dominated by an organic fraction resulting in a calculated hygroscopicity of 0.25±0.05.

286   Based on the calculation of cloud droplet number concentration (N_d) and maximum supersaturation (S_{max}),

287   we find that on a regional scale, most of the variability of N_d is due to the fluctuations in N_a (Table 4), in

288   accordance with other recent studies (Fanourgakis et al., 2019). Nonetheless, N_d levels are also sensitive to

289   fluctuations in σ_w, as a variation by a factor of 4.0 in σ_w may lead to an N_d variation of almost a factor of

290   3.6 and at the same time the N_d response to different N_a levels may be enhanced by a factor of 5 (Figure 4).

291   S_{max} changes in response to aerosol concentration, in a way that tends to partially mitigate N_d responses to

292   aerosol. Overall, maximum supersaturation levels remain quite low (0.14±0.05%) with predicted levels

293   being much lower in lower altitudes (0.05±0.1%). Because of the strong competition for water vapor

294   (expressed by the low S_{max}), cloud droplet number exhibits enhanced sensitivity to aerosol number

295 variations throughout the flights, regardless of aerosol composition. On the other hand, droplet

296 concentration especially within the boundary layer approaches a "plateau" that is strongly driven by vertical

297 velocity (turbulence) and the resulting supersaturation, but also aerosol concentration. In "cleaner"

298 environments where total aerosol number is lower, the relative contribution of vertical velocity to cloud

299 droplet number is almost half during nighttime (24% vs. 42% during daytime) while the relative

300 contribution of N_a to the variance in N_d is somewhat higher (69% vs. 51% during daytime) even though N_a

301 is 2-fold lower during night. On the contrary, in environments with elevated concentrations of

302 accumulation-mode particles, the majority of cloud droplet number variations (54% during nighttime vs.

303 76% during daytime) can be attributed to changes in total aerosol number and to a lesser extent to vertical

304 velocity (43% during nighttime vs. 17% during daytime). The relative contribution of the total aerosol

305 number to the cloud droplet number dominates over variations in chemical composition (expressed by κ).

306 There are cases however where chemical composition variability contributes a non-negligible (~9%)

307 contribution to droplet number variability.

308 Overall, our results show that atmospheric dynamics is a key driver of cloud droplet formation and its

309 variability in the region. Especially in cases when the boundary layer turbulence is low (e.g. during

310 nighttime), low vertical velocity, generating only small supersaturation, can be as important a contributor

311 to droplet number variability as aerosol number. For cases with high vertical velocities and high aerosol

312 number concentration, it is the aerosol concentration that dominates the variability in cloud droplet number.

313 On average, the two variables (N_a and σ_w) contribute almost equally to the variability in cloud droplet

314 number concentration (N_d) and together account for more than 90% of variability. This finding is consistent

315 with recent modeling studies noting the importance of vertical velocity variability as a driver of the temporal

316 variability of global hydrometeor concentration (Morales Betancourt and Nenes, 2014b; Sullivan et al.,

317 2016). Furthermore, the N_d enhancement from changes in N_a is magnified up to 5 times from concurrent

318 changes in σ_w. A similar situation has also been observed in smoke-influenced marine boundary layers in

319 the S.Atlantic (Kacarab et al., 2020). Altogether, these findings carry important implications for model

320 assessments of aerosol indirect climate forcing (e.g., Leibensperger et al., 2012a) and aerosol-cloud

321 interaction studies using remote sensing, as patterns of cooling (although consistent with aerosol and cloud

322 fields) may omit the covariance of vertical velocity with aerosol number, therefore neglecting this important

323 driver of hydrometeor variability.

324 **Data Availability:** The data used in this study can be downloaded from the NOAA public data repository

325 at https://www.esrl.noaa.gov/csd/projects/senex/. The Gaussian fits used for determining σ_w and the droplet

326 parameterization used for the calculations in the study are available from athanasios.nenes@epfl.ch upon

327 request.

339   **Conflicts of Interest:** The authors declare no conflict of interest.

340

341   **References**

342   Barahona, D., West, R.E.L., Stier, P., Romakkaniemi, S., Kokkola, H., and Nenes, A.: Comprehensively

343   accounting for the effect of giant CCN in cloud activation parameterizations, Atmos. Chem. Phys., 10,

344   2467–2473, doi:10.5194/acp-10-2467-2010, 2010.

345   Bougiatioti, A., Bezantakos, S., Stavroulas, I., Kalivitis, N., Kokkalis, P., Biskos, G., Mihalopoulos, N.,

346   Papayannis, A., and Nenes, A.: Biomass-burning impact on CCN number, hygroscopicity and cloud

347   formation during summertime in the eastern Mediterranean, Atmos. Chem. Phys., 16, 7389–7409,

348   https://doi.org/10.5194/acp-16-7389-2016, 2016.

349   Bougiatioti, A., Argyrouli, A., Solomos, S., Vratolis, S., Eleftheriadis, K., Papayannis, A., and Nenes, A.:

350   CCN activity, variability and influence on droplet formation during the HygrA-Cd campaign in

351   Athens, Atmosphere, 8, 108, https://doi.org/10.3390/atmos8060108, 2017.

352   Brock, C. A., Cozic, J., Bahreini, R., Froyd, K. D., Middlebrook, A. M., McComiskey, A., Brioude, J.,

353   Cooper, O. R., Stohl, A., Aikin, K. C., de Gouw, J. A., Fahey, D. W., Ferrare, R. A., Gao, R. S., Gore,

354   W., Holloway, J. S., Hübler, G., Jefferson, A., Lack, D. A., Lance, S., Moore, R. H., Murphy, D. M.,

355   Nenes, A., Novelli, P. C., Nowak, J. B., Ogren, J. A., Peischl, J., Pierce, R. B., Pilewskie, P., Quinn,

356   P. K., Ryerson, T. B., Schmidt, K. S., Schwarz, J. P., Sodemann, H., Spackman, J. R., Stark, H.,

357   Thomson, D. S., Thornberry, T., Veres, P., Watts, L. A., Warneke, C., and Wollny, A. G.:

358   Characteristics, sources, and transport of aerosols measured in spring 2008 during the aerosol,

359   radiation, and cloud processes affecting Arctic Climate (ARCPAC) Project, Atmos. Chem. Phys., 11,
360   2423–2453, 2011.
361 Brock, C. A., Wagner, N. L., Anderson, B. E., Attwood, A. R., Beyersdorf, A., Campuzano-Jost, P.,
362   Carlton, A. G., Day, D. A., Diskin, G. S., Gordon, T. D., Jimenez, J. L., Lack, D. A., Liao, J., Markovic,
363   M. Z., Middlebrook, A. M., Ng, N. L., Perring, A. E., Richardson, M. S., Schwarz, J. P., Washenfelder,
364   R. A., Welti, A., Xu, L., Ziemba, L. D., and Murphy, D. M.: Aerosol optical properties in the
365   southeastern United States in summer – Part 1: Hygroscopic growth, Atmos. Chem. Phys., 16, 4987-
366   5007, https://doi.org/10.5194/acp-16-4987-2016, 2016a.
367 Canagaratna, M. R., Jayne, J. T., Jimenez, J. L., Allan, J. D., Alfarra,M. R., Zhang, Q., Onasch, T. B.,
368   Drewnick, F., Coe, H., Middlebrook, A., Delia, A., Williams, L. R., Trimborn, A. M., Northway, M.
369   J., DeCarlo, P. F., Kolb, C. E., Davidovits, P., and Worsnop, D. R.: Chemical and microphysical
370   characterization of ambient aerosols with the aerodyne aerosol mass spectrometer, Mass Spectrometry
371   Reviews, 26, 185–222, 2007.
372 Carlton, A.G., J.A. de Gouw, J.L. Jimenez, J.L. Ambrose, A.R. Attwood, S. Brown, K.R. Baker, C. Brock,
373   R.C. Cohen, S. Edgerton, C. Farkas, D. Farmer, A.H. Goldstein, L. Gratz, A. Guenther, S. Hunt, L.
374   Jaeglé, D.A. Jaffe, J. Mak, C. McClure, A. Nenes, T.K.V. Nguyen, J.R. Pierce, S. de Sa, N.E. Selin,
375   V. Shah, S. Shaw, P.B. Shepson, S. Song, J. Stutz, J. Surratt, B.J. Turpin, C. Warneke, R.A.
376   Washenfelder, P.O. Wennberg, and Xianling Zhou: A synthesis of the southeast atmosphere studies:
377   coordinated investigation of fundamental atmospheric chemistry questions, Bulletin of the American
378   Meteorological Society, doi: 10.1175-BAMS-D-16-0048.1, 2018.
379 Cubison, M. J., Ervens, B., Feingold, G., Docherty, K. S., Ulbrich, I. M., Shields, L., Prather, K., Hering,
380   S., and Jimenez, J. L.: The influence of chemical composition and mixing state of Los Angeles urban
381   aerosol on CCN number and cloud properties, Atmos. Chem. Phys., 8, 5649-5667,
382   https://doi.org/10.5194/acp-8-5649-2008, 2008.
383 DeCarlo, P. F., Kimmel, J. R., Trimborn, A., Northway, M. J., Jayne, J. T., Aiken, A. C., Gonin, M., Fuhrer,
384   K., Horvath, T., Docherty, K. S., Bates, D. R., and Jimenez, J. L.: Field-Deployable, High-Resolution,
385   Time-of-Flight Aerosol Mass Spectrometer, Anal. Chem., 78, 8281–8289, doi:8210.1021/ac061249n,
386   2006.
387 Fanourgakis, G. S., Kanakidou, M., Nenes, A., Bauer, S. E., Bergman, T., Carslaw, K. S., Grini, A.,
388   Hamilton, D. S., Johnson, J. S., Karydis, V. A., Kirkevåg, A., Kodros, J. K., Lohmann, U., Luo, G.,
389   Makkonen, R., Matsui, H., Neubauer, D., Pierce, J. R., Schmale, J., Stier, P., Tsigaridis, K., van Noije,
390   T., Wang, H., Watson-Parris, D., Westervelt, D. M., Yang, Y., Yoshioka, M., Daskalakis, N., Decesari,
391   S., Gysel-Beer, M., Kalivitis, N., Liu, X., Mahowald, N. M., Myriokefalitakis, S., Schrödner, R.,
392   Sfakianaki, M., Tsimpidi, A. P., Wu, M., and Yu, F.: Evaluation of global simulations of aerosol

393   particle and cloud condensation nuclei number, with implications for cloud droplet formation, Atmos.
394   Chem. Phys., 19, 8591–8617, https://doi.org/10.5194/acp-19-8591-2019, 2019.
395 Fry, J. L., Brown, S. S., Middlebrook, A. M., Edwards, P. M., Campuzano-Jost, P., Day, D. A., Jimenez,
396   J. L., Allen, H. M., Ryerson, T. B., Pollack, I., Graus, M., Warneke, C., de Gouw, J. A., Brock, C. A.,
397   Gilman, J., Lerner, B. M., Dubé, W. P., Liao, J., and Welti, A.: Secondary organic aerosol (SOA)
398   yields from NO3 radical + isoprene based on nighttime aircraft power plant plume transects, Atmos.
399   Chem. Phys., 18, 11663-11682, https://doi.org/10.5194/acp-18-11663-2018, 2018.
400 Cerully, K. M., Bougiatioti, A., Hite, Jr., J. R., Guo, H., Xu, L., Ng, N. L., Weber, R., and Nenes, A.: On
401   the link between hygroscopicity, volatility, and oxidation state of ambient and water-soluble aerosols
402   in the southeastern United States, Atmospheric Chemistry and Physics, 15, 8679–8694, 2015.
403 IPCC (Intergovernmental Panel on Climate Change): Climate Change 2013: The Physical Science Basis,
404   Summary for Policymakers, Cambridge University Press, Cambridge, UK and New York, 2013.
405 Kacarab, M., Thornhill, K. L., Dobracki, A., Howell, S. G., O'Brien, J. R., Freitag, S., Poellot, M. R., Wood,
406   R., Zuidema, P., Redemann, J., and Nenes, A.: Biomass burning aerosol as a modulator of the droplet
407   number in the southeast Atlantic region, Atmos. Chem. Phys., 20, 3029–3040,
408   https://doi.org/10.5194/acp-20-3029-2020, 2020.
409 Kalkavouras, P., Bossioli, E., Bezantakos, S., Bougiatioti, A., Kalivitis, N., Stavroulas, I., Kouvarakis, G.,
410   Protonotariou, A. P., Dandou, A., Biskos, G., Mihalopoulos, N., Nenes, A., and Tombrou, M.: New
411   particle formation in the southern Aegean Sea during the Etesians: importance for CCN production
412   and cloud droplet number, Atmos. Chem. Phys., 17, 175-192, https://doi.org/10.5194/acp-17-175-
413   2017, 2017.
414 Kalkavouras, P., Bougiatioti, A., Kalivitis, N., Stavroulas, I., Tombrou, M., Nenes, A., and Mihalopoulos,
415   N.: Regional new particle formation as modulators of cloud condensation nuclei and cloud droplet
416   number in the eastern Mediterranean, Atmos. Chem. Phys., 19, 6185–6203,
417   https://doi.org/10.5194/acp-19-6185-2019, 2019.
418 Kupc, A., Williamson, C., Wagner, N. L., Richardson, M., and Brock, C. A.: Modification, calibration, and
419   performance of the Ultra-High Sensitivity Aerosol Spectrometer for particle size distribution and
420   volatility measurements during the Atmospheric Tomography Mission (ATom) airborne campaign,
421   Atmos. Meas. Tech., 11, 369–383, https://doi.org/10.5194/amt-11-369-2018, 2018.
422 Lathem, T. L., Beyersdorf, A. J., Thornhill, K. L., Winstead, E. L., Cubison, M. J., Hecobian, A., Jimenez,
423   J. L., Weber, R. J., Anderson, B. E., and Nenes, A.: Analysis of CCN activity of Arctic aerosol and
424   Canadian biomass burning during summer 2008, Atmos. Chem. Phys., 13, 2735-2756,
425   https://doi.org/10.5194/acp-13-2735-2013, 2013.

Atmospheric
Chemistry
and Physics
Discussions

426 Leibensperger, E. M., Mickley, L. J., Jacob, D. J., Chen, W.-T., Seinfeld, J. H., Nenes, A., Adams, P. J.,
427   Streets, D. G., Kumar, N., and Rind, D.: Climatic effects of 1950–2050 changes in US anthropogenic
428   aerosols – Part 1: Aerosol trends and radiative forcing, Atmos. Chem. Phys., 12, 3333-3348,
429   https://doi.org/10.5194/acp-12-3333-2012, 2012a.
430 Leibensperger, E. M., Mickley, L. J., Jacob, D. J., Chen, W.-T., Seinfeld, J. H., Nenes, A., Adams, P. J.,
431   Streets, D. G., Kumar, N., and Rind, D.: Climatic effects of 1950–2050 changes in US anthropogenic
432   aerosols – Part 2: Climate response, Atmos. Chem. Phys., 12, 3349-3362, https://doi.org/10.5194/acp-
433   12-3349-2012, 2012b.
434 Middlebrook, A. M., Bahreini, R., Jimenez, J. L., and Canagaratna, M. R.: Evaluation of Composition-
435   Dependent Collection Efficiencies for the Aerodyne Aerosol Mass Spectrometer using Field Data,
436   Aerosol Sci. Tech., 46, 258–271, doi.org/10.1080/02786826.2011.620041, 2012.
437 Moore, R. H., Bahreini, R., Brock, C. A., Froyd, K. D., Cozic, J., Holloway, J. S., Middlebrook, A. M.,
438   Murphy, D. M., and Nenes, A.: Hygroscopicity and composition of Alaskan Arctic CCN during April
439   2008, Atmos. Chem. Phys., 11, 11 807–11 825, 2011.
440 Moore, R. H., Cerully, K., Bahreini, R., Brock, C. A., Middlebrook, A. M., and Nenes, A.: Hygroscopicity
441   and composition of California CCN during summer 2010, J. Geophys. Res., 117, 2012.
442 Morales, R. and Nenes, A.: Characteristic updrafts for computing distribution-averaged cloud droplet
443   number, autoconversion rate effective radius, J. Geophys. Res., 115, D18220,
444   doi:10.1029/2009JD013233, 2010.
445 Morales Betancourt, R. and Nenes, A.: Droplet activation parameterization: the population-splitting
446   concept revisited, Geosci. Model Dev., 7, 2345–2357, https://doi.org/10.5194/gmd-7-2345-2014,
447   2014a.
448 Morales Betancourt, R. and Nenes, A.: Understanding the contributions of aerosol properties and
449   parameterization discrepancies to droplet number variability in a global climate model, Atmos. Chem.
450   Phys., 14, 4809-4826, https://doi.org/10.5194/acp-14-4809-2014, 2014b.
451 Nenes, A. and Seinfeld, J.H.: Parameterization of cloud droplet formation in global climate models, J.
452   Geophys. Res, 108, 4415, doi:10.1029/2002JD002911, 2003.
453 Petters, M. D. and Kreidenweis, S. M.: A single parameter representation of hygroscopic growth and cloud
454   condensation nucleus activity, Atmos. Chem. Phys., 7, 1961–1971, doi:10.5194/acp-7-1961-2007,
455   2007.
456 Quinn, P. K., Bates, T. S., Coffman, D. J., and Covert, D. S.: Influence of particle size and chemistry on
457   the cloud nucleating properties of aerosols, Atmos. Chem. Phys., 8, 1029-1042,
458   https://doi.org/10.5194/acp-8-1029-2008, 2008.

459 Reutter, P., Su, H., Trentmann, J., Simmel, M., Rose, D., Gunthe, S. S., Wernli, H., Andreae, M. O., and

460   Pöschl, U.: Aerosol- and updraft-limited regimes of cloud droplet formation: influence of particle

461   number, size and hygroscopicity on the activation of cloud condensation nuclei (CCN), Atmos. Chem.

462   Phys., 9, 7067-7080, https://doi.org/10.5194/acp-9-7067-2009, 2009.

463 Seidel, D. J., Zhang, Y., Beljaars, A., Golaz, J.-C., Jacobson, A. R., and Medeiros, B.: Climatology of the

464   planetary boundary layer over the continental United States and Europe, J. Geophys. Res., 117,

465   D17106, doi:10.1029/2012JD018143, 2013.

466 Seinfeld, J., and Pandis, S.: Atmospheric Chemistry and Physics: From Air Pollution to Climate Change,

467   John Wiley, Hoboken, N. J., 1998.

468 Seinfeld, J. H., Bretherton, C. S., Carslaw, K. S., Coe, H., De- Mott, P. J., Dunlea, E. J., Feingold, G., Ghan,

469   S. J., Guenther, A.B., Kahn, R. A., Kracunas, I. P., Kreidenweis, S. M., Molina, M. J., Nenes, A.,

470   Penner, J. E., Prather, K. A., Ramanathan, V., Ramaswamy, V., Rasch, P. J., Ravishankara, A. R.,

471   Rosenfeld, D., Stephens, G., and Wood R.: Improving Our Fundamental Understanding of the Role of

472   Aerosol-Cloud Interactions in the Climate System, P. Nat. Acad. Sci. USA, 113, 5781–5790,

473   https://doi.org/10.1073/pnas.1514043113, 2016.

474 Sullivan, S.C., Lee, D., Oreopoulos, L., and Nenes, A.: The role of updraft velocity in temporal variability

475   of cloud hydrometeor number, Proc.Nat.Acad.Sci, 113, 21, doi: 10.1073/pnas.1514039113, 2016.

476 Wagner, N. L., Brock, C. A., Angevine, W. M., Beyersdorf, A., Campuzano-Jost, P., Day, D., de Gouw, J.

477   A., Diskin, G. S., Gordon, T. D., Graus, M. G., Holloway, J. S., Huey, G., Jimenez, J. L., Lack, D. A.,

478   Liao, J., Liu, X., Markovic, M. Z., Middlebrook, A. M., Mikoviny, T., Peischl, J., Perring, A. E.,

479   Richardson, M. S., Ryerson, T. B., Schwarz, J. P., Warneke, C., Welti, A., Wisthaler, A., Ziemba, L.

480   D., and Murphy, D. M.: In situ vertical profiles of aerosol extinction, mass, and composition over the

481   southeast United States during SENEX and SEAC4RS: observations of a modest aerosol enhancement

482   aloft, Atmos. Chem. Phys., 15, 7085-7102, https://doi.org/10.5194/acp-15-7085-2015, 2015.

483 Warneke, C., Trainer, M., de Gouw, J. A., Parrish, D. D., Fahey, D. W., Ravishankara, A. R., Middlebrook,

484   A. M., Brock, C. A., Roberts, J. M., Brown, S. S., Neuman, J. A., Lerner, B. M., Lack, D., Law, D.,

485   Hübler, G., Pollack, I., Sjostedt, S., Ryerson, T. B., Gilman, J. B., Liao, J., Holloway, J., Peischl, J.,

486   Nowak, J. B., Aikin, K. C., Min, K.-E., Washenfelder, R. A., Graus, M. G., Richardson, M., Markovic,

487   M. Z., Wagner, N. L., Welti, A., Veres, P. R., Edwards, P., Schwarz, J. P., Gordon, T., Dube, W. P.,

488   McKeen, S. A., Brioude, J., Ahmadov, R., Bougiatioti, A., Lin, J. J., Nenes, A., Wolfe, G. M., Hanisco,

489   T. F., Lee, B. H., Lopez-Hilfiker, F. D., Thornton, J. A., Keutsch, F. N., Kaiser, J., Mao, J., and Hatch,

490   C. D.: Instrumentation and measurement strategy for the NOAA SENEX aircraft campaign as part of

491   the   Southeast   Atmosphere   Study   2013,   Atmos.   Meas.   Tech.,   9,   3063-3093,

492   https://doi.org/10.5194/amt-9-3063-2016, 2016.

493   Wilson, J. C., Lafleur, B. G., Hilbert, H., Seebaugh, W. R., Fox, J., Gesler, D. W., Brock, C. A., Huebert,

494   B. J., and Mullen, J.: Function and performance of a low turbulence inlet for sampling supermicron

495   particles from aircraft platforms, Aerosol Sci. Tech., 38, 790–802, 2004.

496   Weber RJ, Guo H, Russell AG, Nenes A.: High aerosol acidity despite declining atmospheric sulfate

497   concentrations over the past 15 years, Nat. Geosci., 9, 282-285, 2016.

498   Yu, S., Alapaty, K., Mathur, R., Pleim, J., Zhang, Y., Nolte, C., Eder, B., Foley, K., and Nagashima, T.:

499   Attribution of the United States "warming hole": Aerosol indirect effect and precipitable water vapor.

500   Sci. Rep., 4, 6929, https:// doi.org/10.1038/srep06929, 2014.

Atmospheric
Chemistry
and Physics
Discussions
Open Access
EGU

501   **Table 1:** Research flights from SENEX 2013 used in this study.

Flight	Date	Local Time (CDT, UTC-5 hrs)	κ	Organic mass fraction
4	10/6	09:55-16:30	0.23±0.02	0.62±0.11
5	11/6	11:30-17:57	0.20±0.00	0.68±0.05
6	12/6	09:48-15:31	0.21±0.01	0.68±0.07
9	19/6	17:30-23:29	0.24±0.01	0.66±0.06
10	22/6	10:01-17:09	0.21±0.02	0.68±0.08
11	23/6	10:08-17:22	0.25±0.03	0.58±0.07
12	25/6	10:18-17:25	0.39±0.02	0.35±0.18
14	29/6	10:26-17:39	0.22±0.03	0.62±0.07
15	2/7	20:08-02:51	0.28±0.05	0.55±0.09
16	3/7	19:56-02:55	0.22±0.05	0.67±0.09
17	5/7	09:52-16:24	0.23±0.05	0.59±0.14
18	6/7	09:19-16:18	0.31±0.02	0.52±0.08
19	8/7	10:11-16:44	0.23±0.04	0.62±0.08

502

503

504

505 **Table 2:** Flight number, time interval, spectral dispersion of vertical wind velocity (σ_w) and characteristic
506 vertical velocity $w^*=0.79\sigma_w$ during flight segments where the aircraft flew at a constant altitude.

Flight (pass)	Time Range	σ_w (m s^{-1})	w^* (m s^{-1})	Altitude (m)	Flight (pass)	Time Range	σ_w (m s^{-1})	w^* (m s^{-1})	Altitude (m)
5 (1)	12:31-12:58	1.02	0.81	549± 58	9 (1)	18:44-18:58	0.255	0.202	797±2.01
5 (2)	13:16-13:29	0.82	0.65	982±11	9 (2)	19:20-19:29	0.249	0.197	740±1.23
5 (3)	13:34-13:50	1.01	0.80	502±13	9 (3)	19:33-19:48	0.217	0.171	740±1.23
5 (4)	13:53-14:08	1.03	0.81	614±27	9 (4)	19:51-20:25	0.218	0.173	776±1.22
5 (5)	14:20-15:00	0.91	0.72	603±40	9 (5)	20:34-20:39	0.232	0.183	597±1.19
5 (6)	15:35-15:41	0.87	0.69	533±18	9 (7)	20:56-21:10	0.201	0.158	773±1.11
5 (7)	16:17-16:30	0.77	0.61	638±23	9 (8)	21:31-21:45	0.191	0.151	725±1.18
5 (8)	16:31-16:39	0.55	0.44	559±18	9 (9)	22:24-22:31	0.257	0.203	745± 1.36
5 (9)	17:10-17:22	0.53	0.42	686±40	9 (10)	22:48-22:54	0.221	0.175	804± 1.37
14 (1)	12:34-12:49	0.94	0.75	558±2	15 (1)	21:09-21:52	0.236	0.186	505±6.64
14 (2)	13:57-14:17	0.97	0.77	658±3	15 (2)	22:19-22:31	0.301	0.238	633±1.21
14 (3)	14:22-14:46	0.95	0.75	737±3	15 (3)	22:42-22:54	0.255	0.202	600±1.17
14 (4)	14:58-15:33	0.55	0.43	746±23	15 (4)	23:26-23:37	0.329	0.260	908±1.56
14 (5)	15:55-16:08	0.57	0.45	714±3	15 (5)	00:02-00:19	0.297	0.235	1208±1.23
14 (6)	16:11-16:21	0.77	0.61	801±3	15 (6)	00:43-1:08	0.253	0.199	592±1.37
14 (7)	16:33-16:41	0.45	0.35	793± 2	15 (7)	1:10-1:24	0.276	0.218	676±1.02
					15 (8)	1:37-2:02	0.207	0.164	713±19.5
12 (1)	11:50-12:34	0.96	0.75	484±3	19 (1)	11:20-11:41	0.622	0.492	1014±2.27
12 (2)	12:48-13:18	1.09	0.86	503±3	19 (2)	12:09-12:23	1.203	0.95	652±3.34
12 (3)	13:34-13:50	1.12	0.88	894±3	19 (3)	12:51-13:10	0.873	0.689	537±2.51
12 (4)	14:06-14:40	1.04	0.82	479±4	19 (4)	13:22-13:49	1.294	1.022	518±22.6
12 (5)	15:21-15:32	1.10	0.87	521±3	19 (5)	14:44-14:57	1.361	1.075	528±3.26
12 (6)	15:43-16:02	0.99	0.78	475±3	19 (6)	15:04-16:06	0.896	0.708	524±2.8

507

508

509 **Table 3:** Derived cloud parameters (maximum supersaturation, droplet number) and relative contribution of chemical composition and total
510 aerosol number for different vertical velocities. Numbers in parentheses indicate standard deviation values.

511

Flight	N_a	N_a variab	$\sigma_w=0.1$ m s^{-1}				$\sigma_w=0.3$ m s^{-1}				$\sigma_w=0.6$ m s^{-1}				$\sigma_w=1.0$ m s^{-1}			
			S_{max}	N_d	Cont κ	Cont N_a	S_{max}	N_d	Cont κ	Cont N_a	S_{max}	N_d	Cont κ	Cont N_a	S_{max}	N_d	Cont κ	Cont N_a
4	6118	4520	0.11 (0.06)	122 (41)	0.08	0.92	0.16 (0.09)	315 (114)	0.20	0.80	0.21 (0.12)	520 (212)	0.23	0.77	0.26 (0.17)	737 (321)	0.2	0.8
5	4324	2598	0.08 (0.04)	139 (31)	0.09	0.91	0.1 (0.06)	388 (104)	0.15	0.85	0.14 (0.08)	712 (216)	0.17	0.83	0.17 (0.1)	1063 (360)	0.21	0.79
6	4958	3054	0.07 (0.07)	151 (24)	0.03	0.97	0.08 (0.04)	422 (70)	0.11	0.89	0.1 (0.06)	773 (171)	0.08	0.92	0.13 (0.07)	1162 (302)	0.07	0.93
9	4271	3095	0.07 (0.02)	152 (18)	0.05	0.95	0.12 (0.04)	367 (68)	0.17	0.83	0.16 (0.05)	533 (115)	0.17	0.83	0.19 (0.06)	680 (126)	0.12	0.88
10	6286	7201	0.07 (0.03)	158 (24)	0.02	0.98	0.1 (0.05)	422 (86)	0.02	0.98	0.14 (0.07)	748 (180)	0.04	0.96	0.18 (0.08)	1063 (295)	0.09	0.91
11	5969	7271	0.04 (0.01)	137 (19)	0.01	0.99	0.06 (0.01)	381 (61)	0.04	0.96	0.08 (0.02)	695 (134)	0.03	0.97	0.10 (0.02)	1025 (226)	0.03	0.97
12	3154	5150	0.06 (0.03)	110 (45)	0.03	0.97	0.1 (0.04)	274 (117)	0.05	0.95	0.14 (0.04)	404 (179)	0.08	0.92	0.17 (0.05)	486 (207)	0.07	0.93
14	5564	5891	0.07 (0.02)	118 (41)	0.05	0.95	0.10 (0.03)	328 (125)	0.17	0.83	0.13 (0.04)	590 (240)	0.25	0.75	0.16 (0.05)	842 (361)	0.27	0.73
15	2328	1428	0.05 (0.01)	135 (22)	0.03	0.97	0.09 (0.02)	339 (67)	0.12	0.88	0.12 (0.02)	557 (137)	0.21	0.79	0.16 (0.03)	717 (203)	0.3	0.7
16	3440	4507	0.08 (0.06)	158 (37)	0.03	0.97	0.12 (0.1)	403 (120)	0.06	0.94	0.17 (0.13)	670 (235)	0.07	0.93	0.23 (0.16)	917 (374)	0.1	0.9
17	3813	4645	0.05 (0.02)	129 (41)	0.06	0.94	0.07 (0.03)	342 (130)	0.1	0.9	0.1 (0.04)	593 (248)	0.06	0.94	0.13 (0.05)	841 (371)	0.06	0.94
18	1925	983	0.08 (0.04)	90 (58)	0.12	0.88	0.12 (0.05)	233 (157)	0.35	0.65	0.15 (0.06)	379 (262)	0.37	0.63	0.19 (0.07)	499 (346)	0.27	0.73
19	4323	7261	0.06 (0.02)	121 (33)	0.02	0.98	0.08 (0.02)	314 (96)	0.06	0.94	0.12 (0.03)	526 (177)	0.11	0.89	0.15 (0.03)	670 (249)	0.13	0.87

512

513

Atmospheric
Chemistry
and Physics
Discussions

514 **Table 4:** Derived S_{max}, N_d, σ_w for all research flights along with the estimated contribution of each
515 parameter to the variability of the droplet number.

Flight	σ_w (m s⁻¹)	$\dfrac{\Delta\sigma_w}{\sigma_w}$	S_{max} (%)	N_d (cm⁻³)	$\dfrac{\Delta N_d}{N_d}$	Contrib. κ	Contrib. N_a	Contrib. σ_w
4	1.03±0.25	0.243	0.29±0.19	707±343	0.485	4%	79%	17%
5	0.97±0.1	0.103	0.17±0.10	1040±350	0.337	7%	69%	24%
6	0.94±0.18	0.191	0.13±0.07	1108±283	0.255	3%	54%	43%
9	0.23±0.02	0.043	0.10±0.03	309±51	0.165	7%	76%	17%
10	1.22±0.11	0.090	0.12±0.03	1177±271	0.230	1%	90%	9%
11	1.08±0.04	0.037	0.11±0.03	1082±242	0.224	1%	83%	16%
12	1.05±0.07	0.067	0.18±0.05	495±210	0.424	2%	96%	2%
14	0.85±0.2	0.024	0.15±0.04	761±321	0.422	9%	72%	19%
15	0.28±0.04	0.143	0.08±0.02	321±63	0.196	7%	51%	42%
16	0.20±0.04	0.200	0.10±0.08	289±79	0.273	2%	65%	33%
17	0.71±0.26	0.366	0.15±0.11	742±280	0.377	1%	71%	28%
18	0.90±0.06	0.067	0.31±0.18	538±325	0.604	7%	83%	10%
19	0.99±0.31	0.313	0.15±0.03	699±248	0.355	4%	88%	8%

516

Atmospheric
Chemistry
and Physics
Discussions
Open Access
EGU
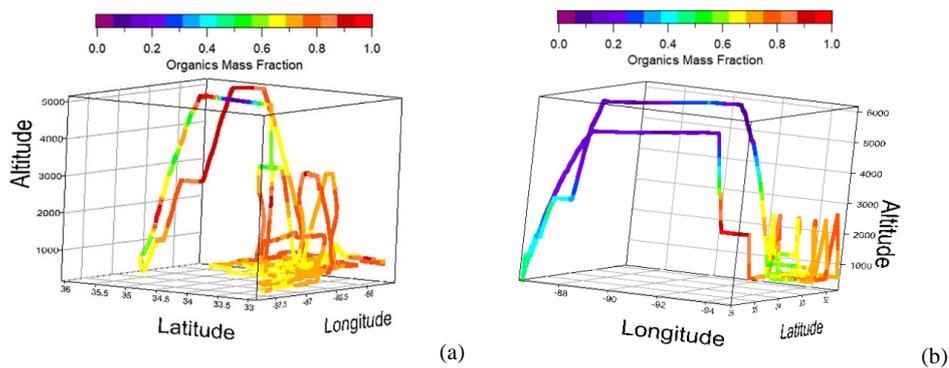
Figure 1: Spatial and vertical distribution of the organics mass fraction (a) for Flight 5 and (b) for Flight 12, denoting the difference in chemical composition, which in turn, may influence cloud droplet number concentration. The color scale denotes the percentage of the organics mass fraction.
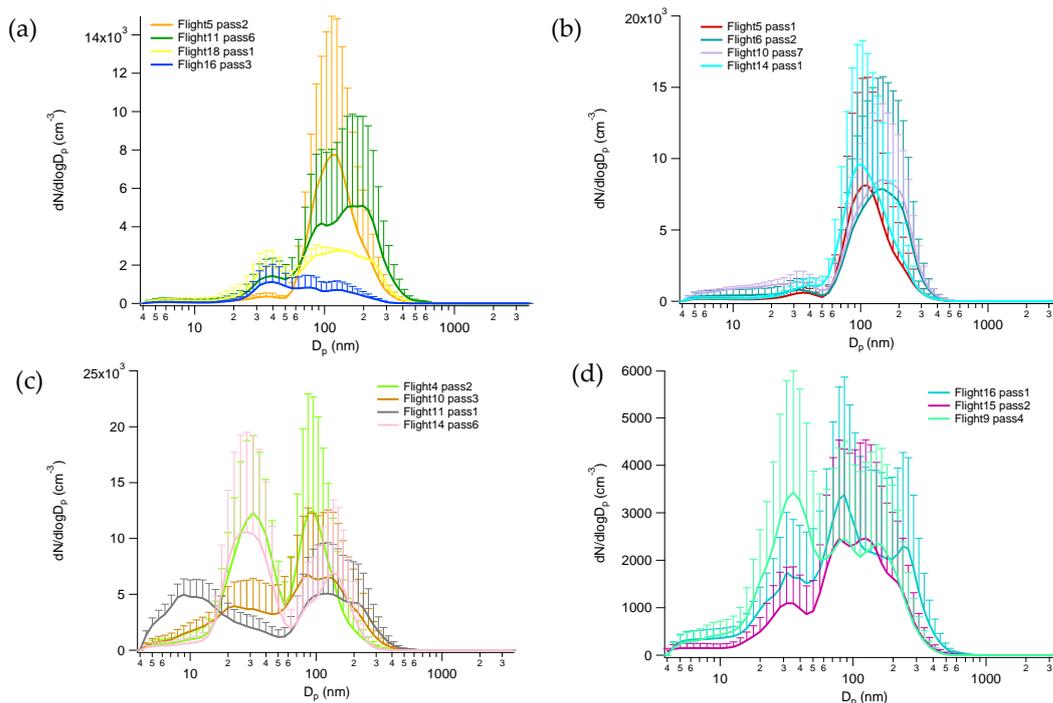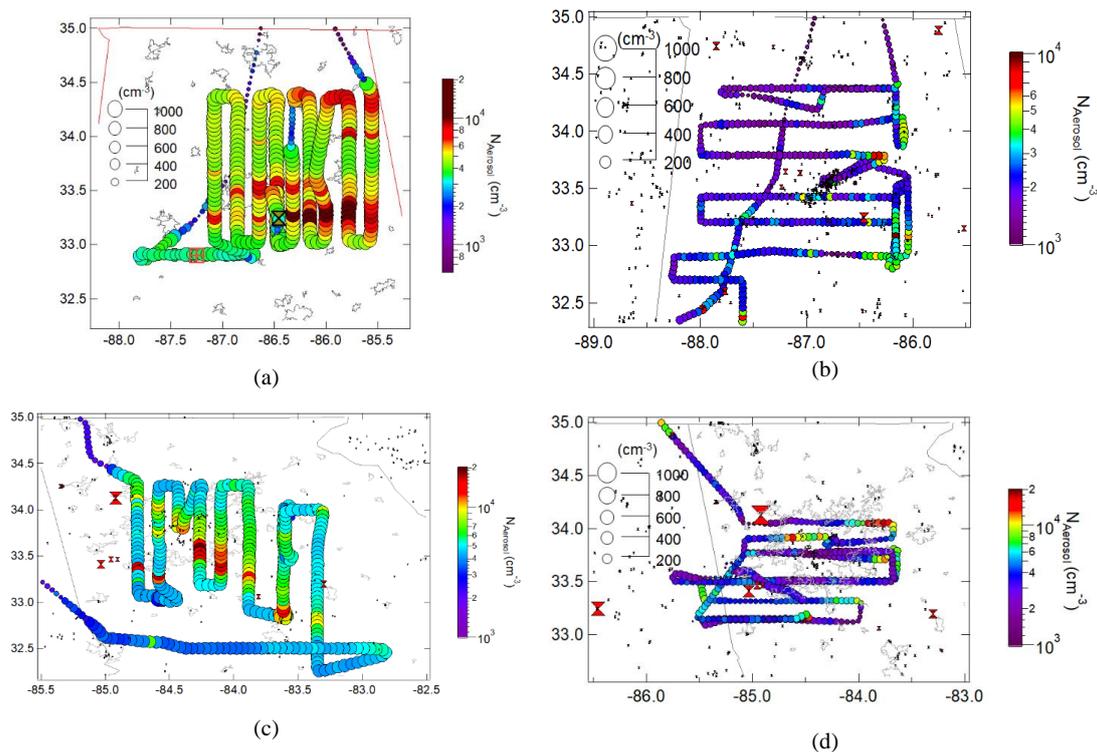
Figure 2: Average particle number size distributions for: (a) free tropospheric conditions, (b) within the boundary layer, (c) for flights with high variability in total aerosol number, and (d) during nighttime flights. Error bars represent the 75th percentile of the distributions within each pass.

526

Figure 3: Flight trajectories showing cloud droplet number (indicated by marker size (cm⁻³)) and total aerosol number (indicated by marker color) for the observed characteristic vertical velocity ($w*$). (a) for the Alabama sector during daytime (Flight 5) and (b) nighttime (Flight 15). (c) for Atlanta during daytime (Flight 6) and (d) nighttime (Flight 9). Note that the data are plotted at less than 1 Hz in order to better show the size and color of the markers.
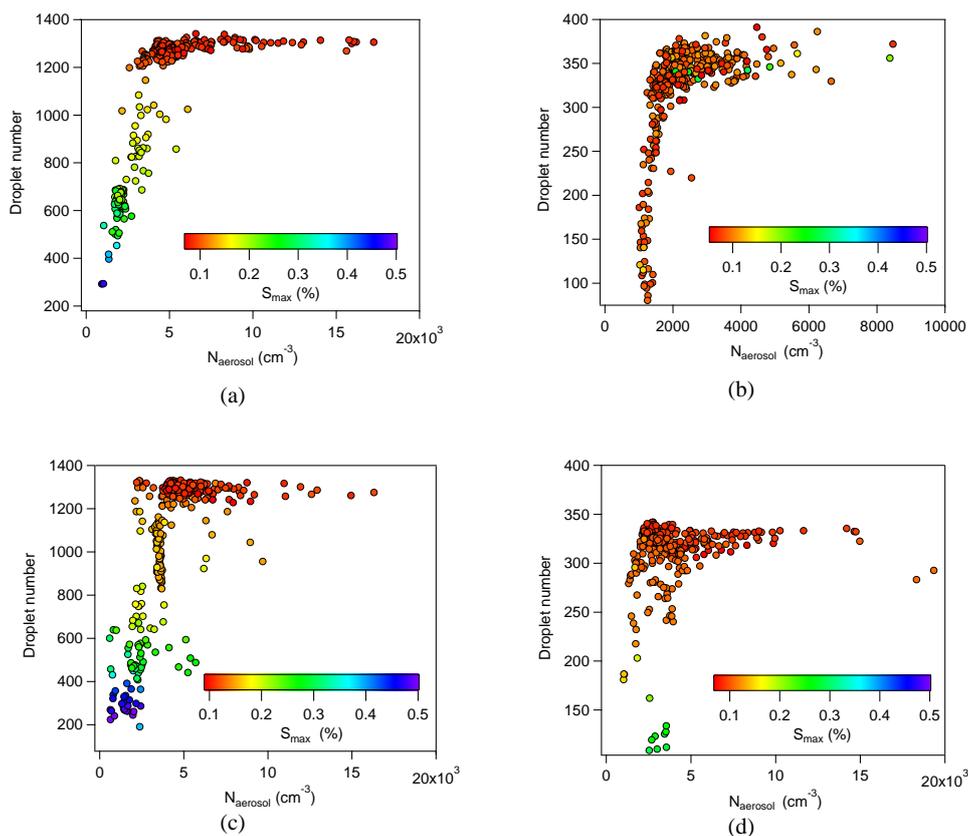
532

533

534

535

536
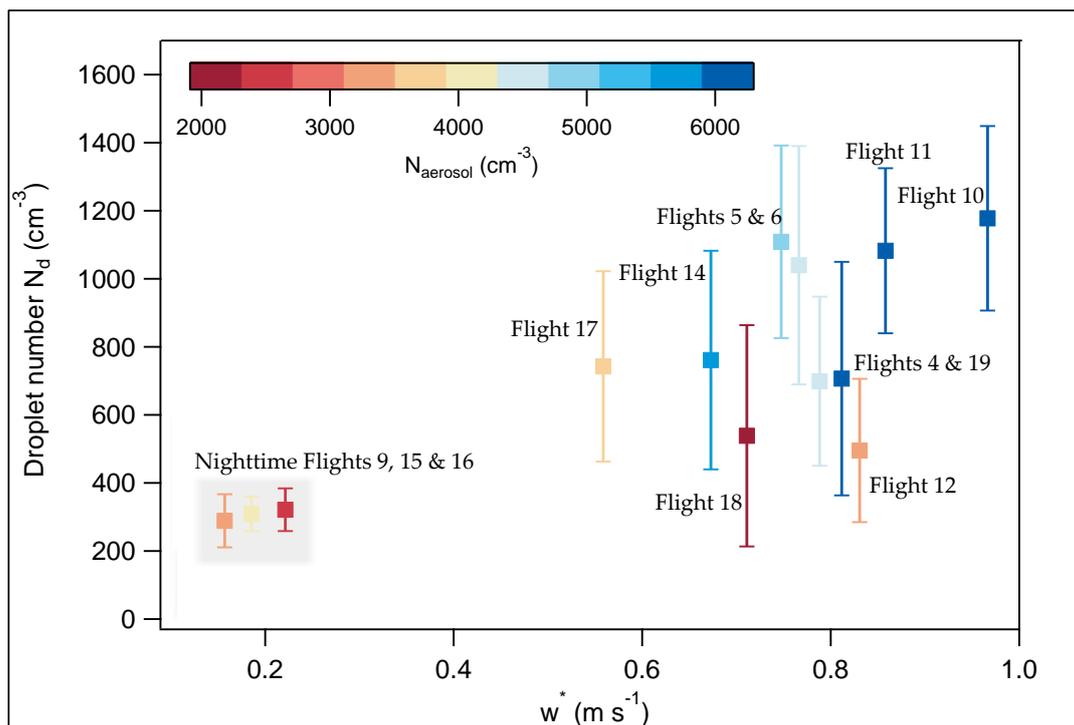
Figure 4: Cloud droplet number vs. total aerosol number for the derived characteristic vertical velocity (w^*). (a) for the Alabama sector during daytime (Flight 5) and (b) nighttime (Flight 15). (c) for Atlanta during daytime (Flight 6) and (d) nighttime (Flight 9). Data are colored by maximum supersaturation.

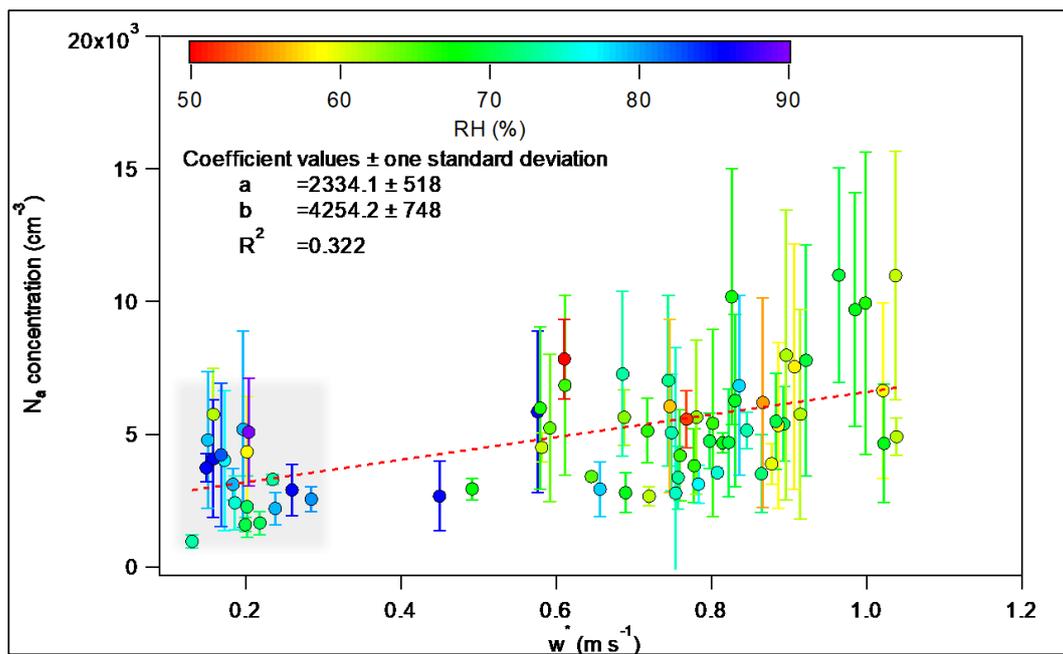544

Figure 5: Average cloud droplet number vs. characteristic velocity during the 13 research flights, colored by total aerosol number. Error bars represent the standard deviation of cloud droplet number during each flight. The shaded area represents the flights conducted during nighttime.

548

549

Figure 6: Total aerosol number vs. characteristic velocity during the segments of the flights when the aircraft remained at a constant altitude within the boundary layer, colored by relative humidity. The shaded area represents the segments of the flights conducted during nighttime.